Supporting Information

Modeling Nanosilver Transformations in Freshwater Sediments

Amy L. Dale[1,2], Gregory V. Lowry[2,3], Elizabeth A. Casman[1,2*]

[1]Engineering and Public Policy, Carnegie Mellon University, Pittsburgh, Pennsylvania

[2]Center for Environmental Implications of Nanotechnology

[3]Civil and Environmental Engineering, Carnegie Mellon University, Pittsburgh, Pennsylvania

*Corresponding author contact information:
E-mail: casman@andrew.cmu.edu
Phone: (412)-268-3756
FAX: (412) 268-3757

14 Pages

6 Supporting Figures

4 Supporting Tables

I. State Variables

Table S1. Model state variables [a]

POC_1	G_1 carbon (most reactive)	g C/g-sed
POC_2	G_2 carbon (less reactive)	g C/g-sed
POC_3	G_3 carbon (unreactive on the timescale considered)	g C/g-sed
O_2	Dissolved oxygen	g O_2/m^3
FeS	Iron sulfide	mol/m^3
FeOOH	Iron oxyhydroxide	mol/m^3
Ag^0	Elemental silver (associated with AgNP)	mol/m^3
Ag_2S (NP)	Silver sulfide (coating particle surface)	mol/m^3
Ag_2S (free)	Silver sulfide (not coating particle surface)	mol/m^3
Ag_T^+	Dissolved (Ag^+) and sorbed (Ag≡POC, Ag≡FeOOH) silver	mol/m^3

[a] The organic carbon concentration is divided into three fractions (f_{POC1}, f_{POC2}, f_{POC3}; see Table 1), each having different reactivity, i.e. ability to be oxidized. This simplification is based on the G model first proposed by Westrich and Berner in 1984[1] and presents a reasonable first approximation of organic carbon diagenesis in sediments.[2] Note that Ag^+ can bind to labile POC, which is included in the model despite not being able to oxidize.

II. Reaction equations

Table S2. Reaction equations and terms[a]

Variable	Reaction	Equation
POC_1	Loss by aerobic oxidation	$R_{POC_1,O_2} = -k_{POC_1,O_2}\theta_{POC_1,O_2}^{(T-20)} \frac{[O_2]}{[O_2]+K_{M,O_2}}[POC_1]$
	Loss by anaerobic oxidation	$R_{POC_1,SO_4} = -k_{POC_1,SO_4}\theta_{POC_1,SO_4}^{(T-20)} \frac{K_{M,O_2}}{[O_2]+K_{M,O_2}}[POC_1]$
POC_2	Loss by aerobic oxidation	$R_{POC_2,O_2} = -k_{POC_2,O_2}\theta_{POC_2,O_2}^{(T-20)} \frac{[O_2]}{[O_2]+K_{M,O_2}}[POC_2]$
	Loss by anaerobic oxidation	$R_{POC_2,SO_4} = -k_{POC_2,SO_4}\theta_{POC_2,SO_4}^{(T-20)} \frac{K_{M,O_2}}{[O_2]+K_{M,O_2}}[POC_2]$
FeS	Gain by anaerobic oxidation of POC	$-a_{FeS,POC}(R_{POC_1,SO_4} + R_{POC_2,SO_4})$
	Loss by oxidation	$R_{FeS,O_2} = -k_{FeS,O_2}\theta_{FeS,O_2}^{(T-20)}[FeS][O_2]$
	Loss by displacement	$a_{FeS,Ag^+}R_{Disp}$
FeOOH	Gain by oxidation of FeS	$-R_{FeS,O_2}$
Ag^0	Loss by oxidation	$R_{Ag^0,O_2} = -k_{Ag^0,O_2}\theta_{Ag^0,O_2}[Ag^0][O_2]$
	Loss by sulfidation	$R_{sulf} = -k_{sulf}[Ag^0][FeS][O_2]$
Ag_2S (NP)	Gain by sulfidation	$-a_{Ag_2S,Ag^0}R_{sulf}$
	Loss by oxidation	$R_{Ag_2S_{NP},O_2} = -k_{Ag_2S,O_2}\theta_{Ag_2S,O_2}^{(T-20)}[Ag_2S(NP)][O_2]$
Ag_2S (free)	Gain by displacement	$-a_{Ag_2S,Ag^+}R_{Disp}$
	Loss by oxidation	$R_{Ag_2S_{free},O_2} = -k_{Ag_2S,O_2}\theta_{Ag_2S,O_2}^{(T-20)}[Ag_2S(free)][O_2]$
Ag^+	Gain by oxidation of Ag^0	$-R_{Ag^0,O_2}$
	Gain by oxidation of Ag_2S (NP)	$-a_{Ag^+,Ag_2S}R_{Ag_2S_{NP},O_2}$
	Gain by oxidation of Ag2S (free)	$-a_{Ag^+,Ag_2S}R_{Ag_2S_{free},O_2}$
	Loss by displacement	$R_{Disp} = -k_{Disp}\{f_{d,Ag^+}(z,t)[Ag_T^+]\}[FeS]$
O_2	Loss by oxidation of POC_1	$a_{O_2,POC}R_{POC_1,O_2}$
	Loss by oxidation of POC_2	$a_{O_2,POC}R_{POC_2,O_2}$
	Loss by oxidation of Ag_2S (NP)	$a_{O_2,Ag_2S}R_{Ag_2S_{NP},O_2}$
	Loss by oxidation of Ag_2S (free)	$a_{O_2,Ag_2S}R_{Ag_2S_{free},O_2}$
	Loss by oxidation of Ag^0	$a_{O_2,Ag^0}R_{Ag^0,O_2}$
	Loss by sulfidation	$a_{O_2,Ag_2S}R_{sulf}$
	Loss by oxidation of FeS	$a_{O_2,FeS}R_{FeS,O_2}$

[a] Reaction equations are of the general form $R_j=k_j\theta_j^{(T-20)}[C_1][C_2]$, where k_j is the reaction rate constant, θ_j is the Arrhenius temperature coefficient, T is the temperature in degrees Celsius, and $[C_1]$ and $[C_2]$ are the concentrations of the reactants. Each reaction is represented by a single R_j: stoichiometric coefficients, denoted $a_{1,2}$, relate R_j to all reactants and products for that equation.

Table S3. Justification of model parameter values in Table 1[a]

Parameter	
General note on Arrhenius temperature coefficients, θ_x: A range of 1.08-1.15 reflects the variation in temperature dependence reported by Di Toro (2001)[3] throughout the text. We assumed the nominal values assumed by Di Toro et al. (1996)[4] [as reported in Di Toro (2001)] in the cadmium sediment model on which this work is based (referred to below as "the Cd model"). The temperature dependence of Ag^0 and Ag_2S oxidation (θ_{Ag^0,O_2} and θ_{Ag_2S,O_2}) was assumed to equal θ_{FeS} and θ_{CdS} from the Cd model.	
General note on organic carbon fractions 1, 2, and 3 and associated oxidation rates: Ranges were based on Table 12.1 and 12.2 of Di Toro (2001), pp. 253-254 (data pooled from 9 sources).	
ϕ_0	Range: See Figure 4.9, p.130 (observed ϕ values pooled from 10 sources)
$k\phi$	Nominal value: Determined by calibration
ρ	Range: See text, p. 4 Nominal value: As in the Cd model
D_d	Range: Table 2.1, p.42 provides an average diffusion coefficient of 1.22(±0.52) cm^2/d. Note that this does not reflect the full natural variability in D_d; Berg et al. (2001) report that bioturbation by sediment-dwelling fauna may double solute transport.[5] In contrast, tortuosity will decrease apparent mixing rates.[6] Nominal value: As in the Cd model
D_p	Range: Min to max values in Table 1, p.1245 (observed values from >30 tracer studies). Note unit conversion. Nominal value: Determined by calibration
z_{D_p}	Range: Min to max values in Table 1, p. 1245 (for mixing depth L; observed values from >30 tracer studies) Nominal value: Represents the reported worldwide mean mixing depth of 9.8 ± 4.5 cm
f_{POC_1}	Range: See general note above on organic carbon fraction and associated oxidation rates Nominal value: As in the Cd model
f_{POC_2}	Nominal value: As in the Cd model
k_{POC_1,O_2}	Nominal value: Rates assumed in the Cd model were an order of magnitude higher than suggested by Table 12.2 of Di Toro (2001) Here, rate constants were chosen to be twice the rate of anaerobic decay.
k_{POC_2,O_2}	Nominal value: Rates chosen to be twice the rate of anaerobic decay
k_{POC_1,SO_4}	Nominal value: Average value reported in Table 12.2 of Di Toro (2001)
k_{POC_2,SO_4}	Nominal value: Average value reported in Table 12.2 of Di Toro (2001)
K_{M,O_2}	Nominal value: As in the Cd model
k_{FeS,O_2}	Range: See Table 21.3, p. 523 and text, p. 521 of Di Toro (2001) (note unit conversions) Nominal case: Calibrated values determined for the Cd model (Experiments 1 and 2) were used. The calibrated value based on the field experiment data (Experiment 3) was not used because it resulted in an unexpectedly low value due to oligotrophic lake conditions.
$k_{Ag^0,O_2}(S/Ag = 0)$	Range: Upper bound is the oxidation rate constant reported for 4.8 nm unsulfidized AgNPs by Liu et al. (2010) adjusted for oxygen-dependence assuming 8 mg/L DO ("air-saturated"). Lower bound is the lowest oxidation rate estimated from the equilibrium solubility of AgNPs reported by Ma et al. (2012) assuming 8.6 mg/L DO (reported). Other estimates from the literature cited fall within this range. Nominal value: Determined by calibration
c_{pass}	Experimental data (Figure 6 from Levard et al. (2011) for AgNP oxidation; Table S3 from Kaegi et al. (2011) for AgNP sulfidation) was fit to the passivation equation (Eq. 13, this work). Values from the fits ranged from 14-21 for AgNP sulfidation and 24 for AgNP oxidation. A representative value of 20 was selected for the nominal case. Although AgNP oxidation and AgNP sulfidation both exhibit surface passivation due to the formation of an Ag_2S shell, the sulfidation rate decreased so rapidly within the first time step after dosing (for a dose of 100% Ag^0 AgNPs) that truncation error due to the finite difference approximation significantly overestimated the rate of both processes (i.e., led to numerical instability). Decreasing the timestep to 3 min greatly increased the model runtime but had no significant effect on model output. The rate of sulfidation was therefore modeled instead as a constant, as described below.
k_{sulf}	Nominal: Liu et al. (2011) report a long-term "second stage" rate of sulfidation of 0.00016 $(mM\ Ag)^{-1}min^{-1}$ for 30 nm AgNPs at pH 11. We assume the DO and sulfide concentrations reported in the text (DO≈0.25 mM, S^{2-}≈1 mM) and a speed-up factor of 3.5 from pH 11 to pH 7 (the factor found by the authors for the "first stage" rate). Range: We assume a lower bound of zero for the sulfidation of a predominantly Ag_2S AgNP sulfidizing by a dissolution-precipitation mechanism (in agreement with the lower bound on Ag_2S oxidation of 0). The upper bound is based on an observation (not reported) that AgNPs sulfidized fully within 4 months during the mesocosm study ($t_{95\%,sulf}$=120 days). Caution should be used if extrapolating these values to other studies. Sulfidation is more accurately represented as a passivation process (e.g., see Eq. 13 in this work). Experimental fits of Table S3 data by Kaegi et al. (2013) assuming the reported DO and sulfide concentrations (Adjusted R^2 values of 0.66-0.96) suggest the *initial* rate of

	sulfidation (e.g., for a fully unsulfidized particle) may be much faster, on the order of 0.041– 0.0086 (mmol S^{2-} /m^3)(mg O_2/m^3)d^{-1} for 10 nm AgNPs and 0.0016–0.00058 (mmol S^{2-}/m^3)(mg O_2/m^3)d^{-1} for a mix of 10-100 nm AgNPs. 100 nm AgNPs showed effectively no sulfidation over 24 hours, revealing the strong size-dependence of the sulfidation rate.
$f_{Ag^0,init}$	Nominal value: Percent sulfidation reported by Kaegi et al. (2011) for AgNPs in the effluent of a pilot WWTP
k_{Ag_2S,O_2}	Derivation: With a forward difference approximation, we see that a first-order rate constant k can be described in terms of the concentration of the reacting chemical species: $$\frac{-\partial C}{\partial t} = kC \Rightarrow k \approx -\frac{1}{C}\frac{C_{t+\Delta t} - C_t}{\Delta t}$$ Multiplying numerator and denominator by a constant volume (and noting that Ag mass is conserved), we see that the rate constant provided by Di Toro et al. (1998)—expressed as (rate of Ag released/mass of Ag present) in units of mg Ag/(g Ag-day)—approximates the more familiar first-order rate constant in units day^{-1} with a simple unit conversion (mg Ag to g Ag). Oxidation rates in Figure 5 (Di Toro et al., 2001) were estimated using the software tool GraphClick (http://www.arizona-software.ch/graphclick/) for the spiked sediment (nominal case) and the sediment core (upper bound). A second-order rate constant was approximated assuming $[O_2]$=8000 mg/L for the values reported. A lower bound of zero was chosen based on the insolubility of Ag_2S.
k_{Disp}	Nominal value: Chosen to match the calibrated value for the three experiments reported in Table 21.3 p. 523. Good agreement was found during calibration to mesocosm data.
$J_{POC,\max}$	Range: POC deposition fluxes were assumed based on observed sedimentation accumulation fluxes and an assumed organic carbon content of settling solids of 20%. Gasiorowski et al. (2008) provide mean sedimentation rates for five shallow lakes in Poland. Rose et al. (2011) provide sediment accumulation rates for 207 European lakes (incl. mountain lakes and lowland lakes). For a eutrophic lake in China, Wan et al. (2005) estimate J_{POC}=160 to 440 mg/m^2-d (note unit conversion) between 1970-1997 with an average value of 270 mg/m^2-d, suggesting that 300 is an acceptable upper limit for a nutrient-enriched system. It was necessary to limit the range of values considered in the model to ensure numerical stability.
$\log K_{OC}$	Range: See Table 4, p. 3-11 for log(K_d) values for Ag^+ partitioning between pore water and sediments (2.1-5.8). We assume all Ag^+ is bound to organic carbon and L.O.I. is 1.83% (value observed in mesocosms, transformed assuming $f_{oc} \approx$ L.O.I./2). From Schwarzenbach et al. (2002), p. 292:[7] $$K_{OC} = \frac{K_d}{f_{oc}}$$
σ_{OC}	Nominal value: Assumed in the Cd model (for cadmium). Benjamin and Leckie (1981) suggest Cd^{2+} and Ag^+ exhibit comparably low critical adsorption densities Γ* for sorption to amorphous iron oxyhydroxides,[8] revealing the two species have similar preferences for a small number of preferred binding sites (Γ* values ordered by metal species: Pb< Ag< Cd < Cu < Hg < Zn < Co). Ag^+ adsorption to mineral species is relatively poorly studied.
K_{FeOOH}	Nominal value: As in the Cd model (for cadmium). Overlapping K_d values were reported for cadmium (mean of 3.3, range of 0.5-7.3) and silver (mean of 3.6, range of 2.1-5.8) by Allison and Allison (2005).[9] Ag^+ and Cd^{2+} preferentially sorb to POC, suggesting this assumption has little impact on the system response.
σ_{FeOOH}	Nominal value: As in the Cd model (for cadmium). See notes for σ_{OC} and K_{FeOOH}
π_{FeS}	Range: Calibrated values calculated in the Cd model (Table 21.3, p. 523). Natural variability in this parameter is likely larger than reported. Nominal value: Calibrated values determined for the Cd model (Experiments 1 and 2)
Initial and Boundary Conditions	
O_2(z=0)	Range: Values represent a range of conditions at the sediment-water interface, from anoxic to oxic
f_{oc}(t=0)	Range: See text, p. 15 of Di Toro et al. (2001) for observed values for coastal marine and harbor sediments. Range agrees with Schwarzebach et al. (2002) (Figure 9.7, p.292).[7] Field studies report L.O.I. values from 1 to 70%. Assuming f_{om}=2*f_{oc} suggests a wider range for f_{oc} of 0.5-0.35, but we do not think it is equally representative. Nominal: Selected from Figure 1.9, p. 16 of Di Toro et al. (2001) to represent a "typical" (non-eutrophic, non-oligotrophic) system.
FeS(t=0)	Range: See Figure 1.9, p.16 of Di Toro (2001) for AVS (acid volatile sulfide) concentrations for coastal marine and harbor sediments. FeS is a proxy for AVS in this model. Nominal value: Selected from Figure 1.9 to represent a "typical" (non-eutrophic, non-oligotrophic) system.

[a]Listed tables, figures, and page numbers correspond with sources cited in Table 1 (main text)

III. Silver Ion Partitioning

The partitioning of the total silver ion concentration ($[Ag_T^+]$) between the dissolved form (Ag^+) and the two sorbed forms (Ag≡POC and Ag≡FeOOH) is governed by the partitioning coefficients K_{OC} and K_{FeOOH}.

$$K_{OC} = \frac{[Ag \equiv POC]}{[Ag^+][\equiv POC]} \quad (S1)$$

$$K_{FeOOH} = \frac{[Ag \equiv FeOOH]}{[Ag^+][\equiv FeOOH]} \quad (S2)$$

where $[\equiv POC]$ and $[\equiv FeOOH]$ are the concentration of available binding sites on the organic carbon and iron oxyhydroxide, respectively.

From these and other principles of solid phase partitioning (see Di Toro *et al*., 1996), the following equations can be derived.

$$[Ag \equiv POC] = \frac{K_{OC}[Ag^+]\sigma_{POC}[POC]}{1 + K_{OC}[Ag^+]} \quad (S3)$$

$$[Ag \equiv FeOOH] = \frac{K_{FeOOH}[Ag^+]\sigma_{FeOOH}[FeOOH]}{1 + K_{FeOOH}[Ag^+]} \quad (S4)$$

where σ_{FeOOH} and σ_{POC} represent the specific binding capacity of the sorbent, such that

$$\sigma_{POC} = \frac{[\equiv POC]_T}{[POC]} \quad \text{and} \quad \sigma_{FeOOH} = \frac{[\equiv FeOOH]_T}{[FeOOH]} \quad (S5, S6)$$

Here, $[\equiv FeOOH]_T$ and $[\equiv POC]_T$ represent the total concentration of binding sites (free and silver-bound).

It can be shown that the dissolved ion concentration is the solution for x in the cubic equation $q_3x^3 + q_2x^2 + q_1x + q_0 = 0$, where $x = [Ag^+]$.

$$\begin{aligned}
q_3 &= K_{FeOOH}K_{OC}\phi \\
q_2 &= K_{FeOOH}K_{OC}(\phi - 1)\rho([\equiv FeOOH]_T + [\equiv POC]_T) \\
&\quad - \phi(K_{FeOOH} + K_{OC}) + K_{FeOOH}K_{OC}[Ag_T^+] \\
q_1 &= K_{OC}(\phi - 1)\rho([\equiv POC]_T) + K_{FeOOH}(\phi - 1)\rho([\equiv FeOOH]_T) \\
&\quad + (K_{FeOOH} + K_{OC})[Ag_T^+] - \phi \\
q_0 &= [Ag_T^+] \qquad (S7)
\end{aligned}$$

IV. Exponential Expanding Finite Difference Grid

The distance between volume elements *i* and *i*+1 in an exponentially expanding finite difference grid expands with overall distance from the top boundary according to the formula:

$$\Delta z_i = \Delta z e^{\beta(i-1)} \quad (S8)$$

where Δz is the thickness of the first volume element and $0<\beta<0.5$ is a constant. In our model, $\beta=0.005$.

The following equations describe the distance between the top boundary (the sediment-water interface) and the inner and outer boundary of each grid volume, respectively.

$$z_i' = \Delta z \frac{e^{\beta(i-1)} - 1}{e^{\beta} - 1} \qquad z_i'' = \Delta z \frac{e^{\beta i} - 1}{e^{\beta} - 1} \quad (S9, S10)$$

The location of the average concentration in each grid volume is described by the following equation:

$$\bar{z}_i = \Delta z \frac{e^{\beta(i-0.5)} - 1}{e^{\beta} - 1} \quad (S11)$$

Note that this point is not located exactly in the center of each volume element (Figure S1). To correct for this, the non-uniform grid is mapped to a uniform grid by adjusting the mixing coefficients D_p and D_d (denoted here as the general term D). In this case, dimensionless diffusion coefficients at the upper and lower boundaries of each grid space are calculated as:

$$D_i' = \frac{D^*}{e^{2\beta(i-0.25)}} \qquad D_i'' = \frac{D^*}{e^{2\beta(i-0.75)}},$$

$$D_1' = D^* \frac{e^{\beta} - 1}{e^{0.5\beta} - 1} \quad (S12 - S14)$$

where $D^* = D\Delta t/\Delta z^2$ is simplifying notation used in the solution to the mass balance equation.

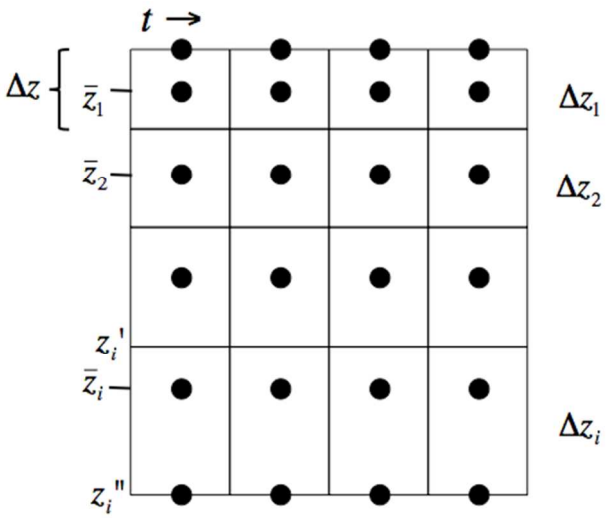

Figure S1. A diagram of the exponentially expanding grid space showing key variables.

As a proof of concept, consider a species C_1 present entirely in either its dissolved or particulate form (f_p=1 or f_d=1) undergoing a single reaction that is first order with respect to two reactants. For a uniform grid, the fully implicit form of the solution to the mass balance equation can be expressed in its simplest form as:

$$C_1(i,n+1) = C_1(i,n) \; + \; \begin{Bmatrix} D*\left\{C_1(i+1,n+1) - C_1(i,n+1)\right\} \\ -D*\left\{C_1(i,n+1) - C_1(i-1,n+1)\right\} \\ -\Delta t k C_1(i,n+1) C_2(i,n+1) \end{Bmatrix} \quad (S15)$$

Note that, in our model, *D*'s are depth-dependent before implementation of the exponentially expanding grid.

For a non-uniform grid, taking into account changes in *z* as well as changes in diffusion coefficients, the solution becomes

$$C_1(i,n+1) = C_1(i,n) \; + \; \Delta t \begin{Bmatrix} \dfrac{D}{\Delta z_i}\left\{\dfrac{C_1(i+1,n+1) - C_1(i,n+1)}{\bar{z}_{i+1} - \bar{z}_i}\right\} \\ -\dfrac{D}{\Delta z_i}\left\{\dfrac{C_1(i,n+1) - C_1(i-1,n+1)}{\bar{z}_i - \bar{z}_{i-1}}\right\} \\ -k C_1(i,n+1) C_2(i,n+1) \end{Bmatrix} \quad (S16)$$

Applying the equations above and simplifying, the solution takes the form:

$$C_1(i,n+1) = C_1(i,n) \; + \; \begin{Bmatrix} D_i''\left\{C_1(i+1,n+1) - C_1(i,n+1)\right\} \\ -D_i'\left\{C_1(i,n+1) - C_1(i-1,n+1)\right\} \\ -\Delta t k C_1(i,n+1) C_2(i,n+1) \end{Bmatrix} \quad (S17)$$

which must be then solved for the unknown concentration at time step n+1, $C_1(i,n+1)$, using the quadratic equation.

A complete treatment of this approach is provided by Feldberg (1981).

VI. Case: Pulse Input

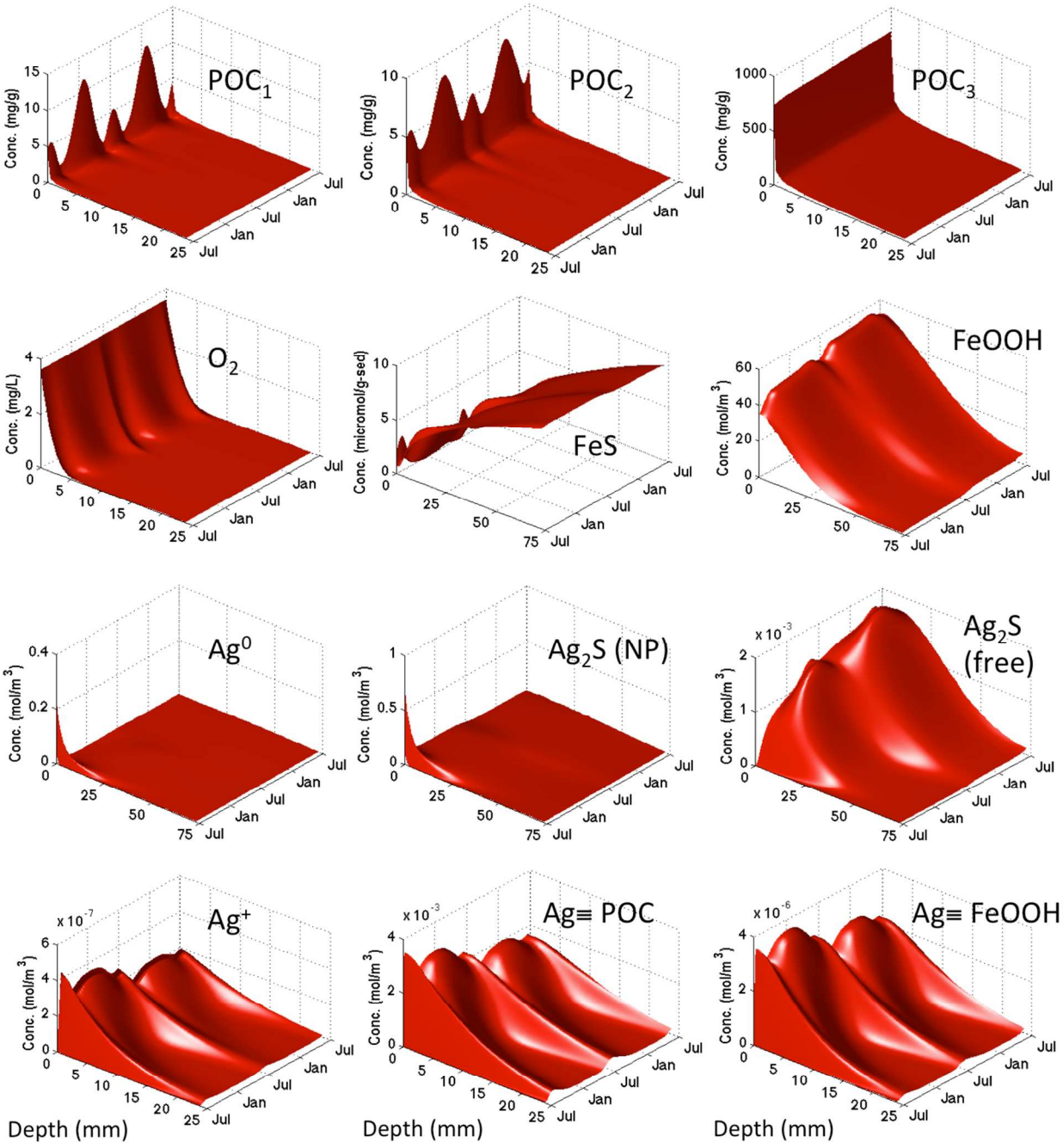

Figure S2. Change in depth profiles of all state variables over time after a pulse input of 2.9 g of 85% sulfidized nanoparticles. Temperature and oxygen availability are anticyclical (oxygen concentration peaks in winter). Since high oxygen concentrations (winter) and high temperatures (summer) both facilitate oxidation, complex periodic behavior results. Natural systems are expected to exhibit more complexity and variability.

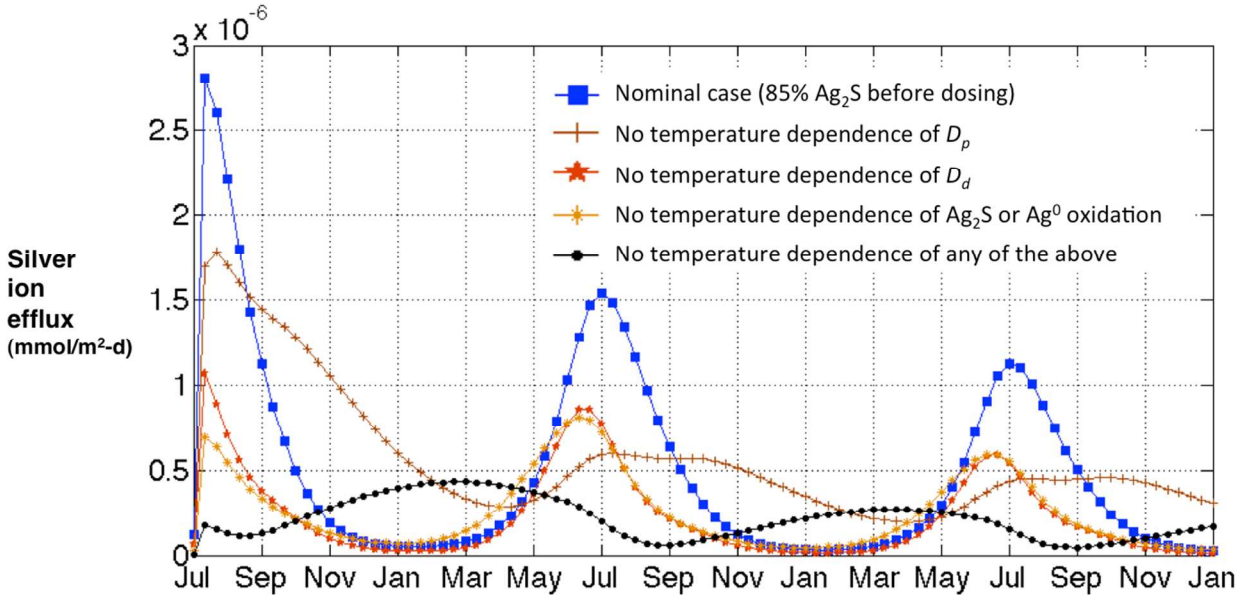

Figure S3. Sensitivity of seasonal trends in Ag^+ efflux to temperature coefficients and oxygen availability. In spite of increased oxygen penetration in winter, the model predicts Ag^+ will peak in summer due to increased oxidation and increased mixing (particulate and dissolved).

Table S4. Model elasticities, ranked from highest to lowest[a]

Symbol	Parameter	Elasticity
θ_{Ag_2S,O_2}	Correction for Arrhenius temperature dependence	16
θ_{D_p}	Correction for Arrhenius temperature dependence	-16
θ_{D_d}	Correction for Arrhenius temperature dependence	9.5
θ_{FeS,O_2}	Correction for Arrhenius temperature dependence	-2.3
θ_{Ag^0,O_2}	Correction for Arrhenius temperature dependence	2.2
ϕ_0	Sediment porosity at the sediment-water interface	2.2
O_2(z=0)	Oxygen concentration at the interface	1.9
f_{oc}(t=0)	Fraction of organic carbon in sediment (at t=0)	-1.3
ρ	Sediment density	-1.1
θ_{POC_2,SO_4}	Correction for Arrhenius temperature dependence	-1.0
k_{Ag_2S,O_2}	Rate of oxidation of sulfur in Ag_2S	0.99
D_p	Particle mixing velocity	-0.87
σ_{OC}	Sorption capacity for POC	-0.86
K_{OC}	Partition coefficient to POC	-0.86
D_d	Molecular diffusion coefficient	0.61
θ_{POC_1,SO_4}	Correction for Arrhenius temperature dependence	-0.58
$J_{POC,\max}$	Flux of organic carbon from the overlying water	-0.46
f_{POC_1}	Fraction of POC in G_1 reactivity class	-0.37
$k\phi$	Rate of decrease in sediment porosity with depth	-0.36
π_{FeS}	Partition coefficient for FeS: $[FeS_p]/[FeS_d]$	0.20
f_{POC_2}	Fraction of POC in G_2 reactivity class	-0.16
k_{FeS,O_2}	Rate of oxidation of FeS to form FeOOH	-0.13
θ_{POC_2,O_2}	Correction for Arrhenius temperature dependence	0.083
k_{POC_2,SO_4}	Rate of anaerobic oxidation of G_2 carbon	-0.060
z_{D_p}	e-folding depth of particle mixing	-0.053
k_{POC_1,O_2}	Rate of aerobic oxidation of G_1 carbon	0.032
k_{POC_1,SO_4}	Rate of anaerobic oxidation of G_1 carbon	-0.028
k_{POC_2,O_2}	Rate of aerobic oxidation of G_2 carbon	0.027
k_{Disp}	Rate of displacement reaction	-0.021
θ_{POC_1,O_2}	Correction for Arrhenius temperature dependence	-0.0040
$f_{Ag^0,init}$	Percent elemental silver by mass in input dose of NPs	0.0038
$k_{Ag^0,O_2}(\%_{Ag}=0)$	Initial rate of nanoparticle dissolution	0.0034
σ_{FeOOH}	Sorption capacity for FeOOH	-0.00093
K_{M,O_2}	Half saturation constant for oxidation using O_2	0.00089
K_{FeOOH}	Partition coefficient to FeOOH	-0.00081
FeS(t=0)	Sediment iron sulfide (AVS) concentration (at t=0)	-0.00057
k_{sulf}	Rate of AgNP sulfidation	0.00039
c_{pass}	Rate of decrease in Ag^0 oxidation rate as a function of S/Ag	0.00

[a] The measured output is the peak concentration of dissolved silver ion in the sediment within six months of dosing. Green shading indicates parameters for which uncertainty stems predominantly from natural variability. Blue shading indicates parameters for which uncertainty stems predominantly from experimental uncertainty in constants or coefficients. The most influential parameters appear to be the temperature coefficients of the reaction and mixing rates. However, the effect of temperature sensitivity on model results is limited by relatively small uncertainty surrounding the true values of these parameters (Table 1). System parameters such as porosity at the interface, ϕ_0,

the initial organic carbon composition of the sediment, f_{oc}(t=0), sediment density, ρ, and the oxygen concentration at the sediment-water interface, O_2(z=0), reveal the importance of sediment redox conditions in determining the extent of nanoparticle oxidation. The most influential reaction rate constants and coefficients are the rate of oxidation of sulfur in silver sulfide, $k_{Ag2S,O2}$, and parameters describing the partitioning behavior of silver ion (the silver ion-organic carbon partition coefficient, K_{OC}, and the sorption capacity for organic carbon, σ_{OC}).

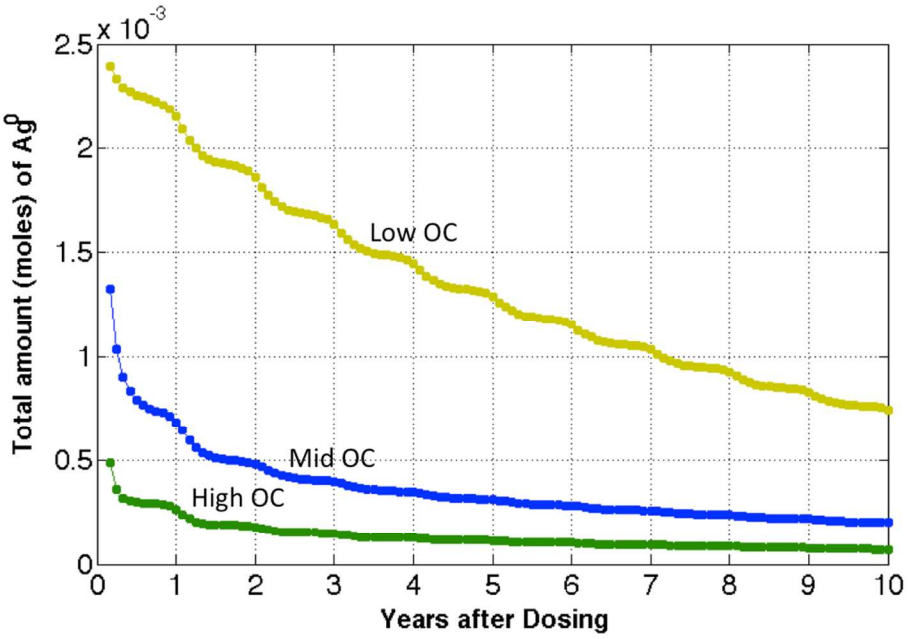

Figure S4. Loss of Ag^0 over time for a pulse input of 85% sulfidized AgNPs. Sulfidation of AgNPs during nanoparticle influx leads to lower peak amounts of Ag^0 in environments with more organic carbon (higher sulfide availability). The cores are affected by two loss processes simultaneously (AgNP oxidation leading to Ag^+ release and sulfidation). The overall loss rate decreases over time, and the first order decay exhibited by the entire transformed AgNP (Figure 4 in main text) is not observed.

VII. Case: Constant Influx of AgNPs

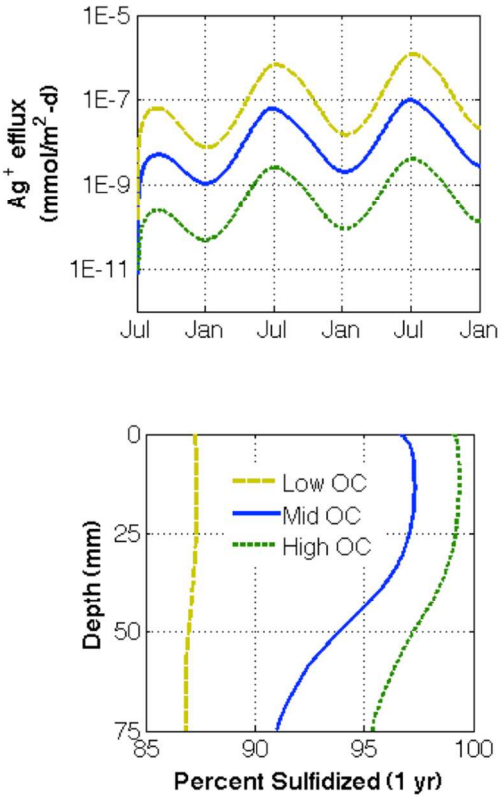

Figure S5. System response to constant inputs of 85% sulfidized nanoparticles (0.03 mg Ag/m^2-d). Compare to Figure 4 in main text. Above: Silver ion efflux vs. time after dosing for low ($J_{POC,max}$=50 mg/m^2-d, f_{oc}=0.001), middle ($J_{POC,max}$=150, f_{oc}=0.02), and high ($J_{POC,max}$=300, f_{oc}=0.15) levels of organic carbon (OC). Silver ion release will be maximized in low carbon environments, which have lower oxygen demand and thus correspond to oxic conditions. The accumulation of AgNPs over time leads to an increase in the formation and efflux of silver ion from the sediment. Below: Percent sulfidation within a year of dosing increases as the organic carbon content of the sediments increases, since sulfide is formed by the degradation of organic carbon in the anoxic sediments.

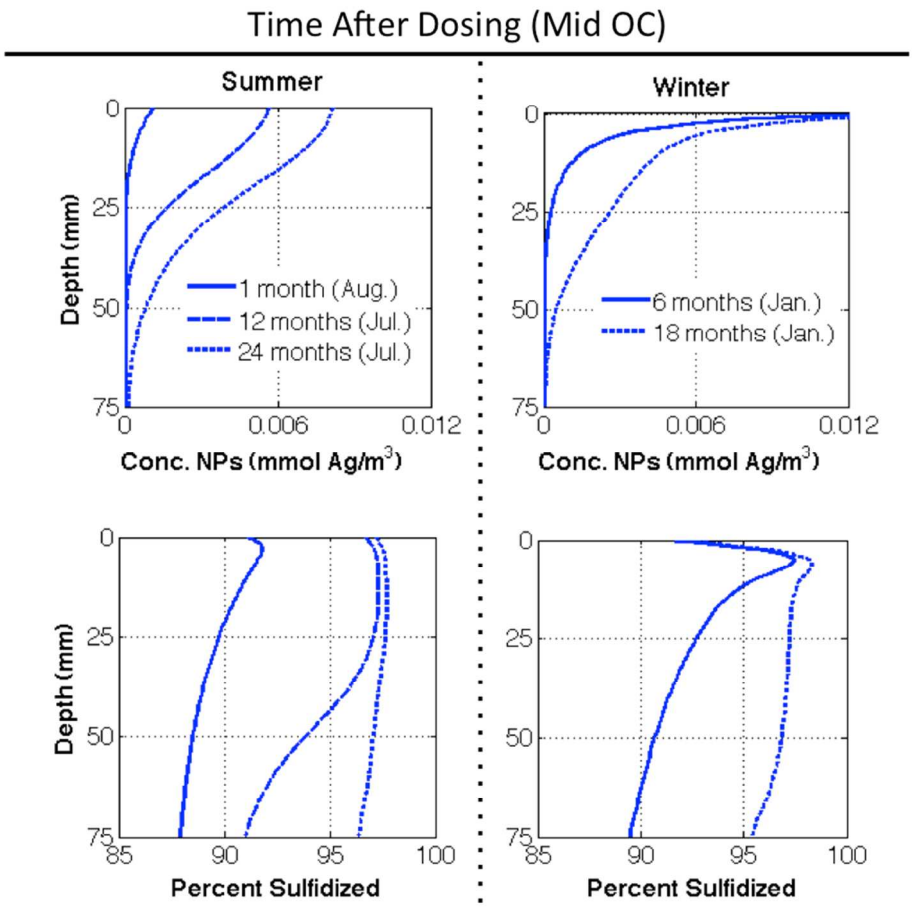

Figure S6. Change in concentration profile (above) and sulfidation (below) of AgNPs in the sediment over time. Results are shown only for the mid OC case ($J_{POC,max}$=150, f_{oc}=0.02). For the concentration profiles, only minor differences are observed between this case and the low/high OC cases because the AgNPs are highly persistent. AgNP concentrations at the interface decrease in summer as a result of increased particle mixing and increased oxidation, which results from higher temperatures. Liu et al. (2011) have shown that AgNP sulfidation requires a strong oxidant, which we assume is dissolved oxygen. Thus there is a greater extent of sulfidation near the oxic sediment-water interface than occurs at depth. The extent of sulfidation drops at the interface, reflecting the less sulfidized nature of the incoming particles.

References

1. Westrich, J. T.; Berner, R. A., The role of sedimentary organic matter in bacterial sulfate reduction: The G model tested. *Limnology and Oceanography* **1984**, 236-249.
2. Boudreau, B. P., *Diagenetic models and their implementation: modelling transport and reactions in aquatic sediments*. Springer Berlin: 1997.
3. Di Toro, D. M., *Sediment flux modeling*. Wiley-Interscience New York: 2001.
4. Di Toro, D. M.; Mahony, J. D.; Hansen, D. J.; Berry, W. J., A model of the oxidation of iron and cadmium sulfide in sediments. *Environmental Toxicology and Chemistry* **1996,** *15*, (12), 2168-2186.
5. Berg, P.; Rysgaard, S.; Funch, P.; Sejr, M. K., Effects of bioturbation on solutes and solids in marine sediments. *Aquatic Microbial Ecology* **2001,** *26*, (1), 81-94.
6. Boudreau, B. P., Metals and models: diagenic modelling in freshwater lacustrine sediments. *Journal of Paleolimnology* **1999,** *22*, (3), 227-251.
7. Schwarzenbach, R. P.; Gschwend, P. M.; Imboden, D. M., *Environmental organic chemistry*. Wiley-Interscience: 2005.
8. Benjamin, M. M.; Leckie, J. O., Multiple-site adsorption of Cd, Cu, Zn, and Pb on amorphous iron oxyhydroxide. *Journal of Colloid and Interface Science* **1981,** *79*, (1), 209-221.
9. Allison, J. D.; Allison, T. L., Partition coefficients for metals in surface water, soil, and waste. *Rep. EPA/600/R-05* **2005,** *74*.